

Graz University of Technology Bachelor's Thesis

OMNIRESONANCE IN THE NEAR-INFRARED

Author: Lorenz Weiß

Matriculation Number: 12121146

Program: BSc Physics

Supervisor: Ass. Prof. Dr.rer.nat. Marcus Ossiander

Submitted on:

22.07.2025

Contents

1	Intr	roduction	4
2	2 Achromatic Resonance Theory		
	2.1	Experiment Design	5
	2.2	Reaching the Target Dispersion	8
3	Exp	perimental Setup	10
	3.1	Components and Equipment	13
	3.2	Construction and Characterization of the Cavity	14
	3.3	Beam Splitter Characterization	15
4	Ach	romatic Resonance Demonstration	16
5	Dis	cussion and Conclusion	19

Abstract

This thesis investigates the realization of achromatic resonance in a Fabry-Pérot cavity, addressing the limitation of conventional resonators that restricts resonance to discrete wavelengths. We implement an approach using a transmission grating and convex lens to generate angular dispersion, allowing each wavelength in a broadband beam to enter the cavity at a specific angle. This configuration compensates the chromatic dependence of the resonance condition, enabling multiple wavelengths to simultaneously satisfy the phase-matching requirement. Theoretical analysis identifies a target angular dispersion, which is approximated experimentally. Spectral transmission measurements confirm the wavelength independence of the resonance features over a 15 nm bandwidth, demonstrating achromatic resonance across nearly three free spectral ranges. The results validate the feasibility of angular-dispersion-based resonance broadening and offer a practical alternative to lossy dispersion-engineered systems.

1 Introduction

Resonators, such as Fabry-Pérot cavities, are widely used in photonics for their ability to enhance light fields based on the interference conditions within a cavity. This enhancement occurs only for discrete wavelengths whose round-trip phase satisfies a strict integer-multiple condition [1]. This inherently wavelength-dependent behavior limits the resonator's applicability in broadband systems, where consistent resonance across a wider spectrum is required.

Several approaches have been explored that aim to overcome this limitation and achieve achromatic resonance. The most common strategy is the use of negatively dispersive materials inside the cavity [2-6]. The refractive index n changes in a way that cancels the natural phase dispersion occurring in the cavity. As a result, the group delay becomes flatter, and the phase accumulation varies more linearly with frequency, allowing multiple wavelengths to fulfill the cavity's resonance condition simultaneously, making it a white-light-cavity. [7]

Naturally, negative dispersion is typically observed only in narrow spectral regions near atomic resonances, but it is accompanied by strong absorption, making it unsuitable for practical applications [8]. To overcome these limitations, a number of approaches have been used, such as electromagnetically induced transparency (EIT) with population inversion [2], coherent Raman scattering [5, 6] or the use of nonlinear Kerr-dispersion [3, 4].

Although effective, these approaches often suffer from narrow resonance bandwidths [2], environmental sensitivity [3, 5] and experimental complexity. Systems based on atomic coherence or nonlinear effects require precise control over parameters like temperature, pump power, and atomic density [4, 5].

In this work, we demonstrate an alternative method for achieving achromatic resonance in a Fabry–Pérot cavity by using a transmission grating and a convex lens to produce inverted angular dispersion. This approach offers a simple and broadband-compatible alternative to traditional intracavity dispersion techniques. By directing each wavelength of a broadband beam into the cavity at a specific angle, the setup compensates for phase shifts and enables multiple wavelengths to resonate simultaneously.

2 Achromatic Resonance Theory

For a resonator consisting of two planar, opposing and parallel mirrors at a distance L, only discrete wavelengths resonate: those whose round trip phase φ in the cavity is an integer multiple of 2π [1],

$$\varphi = 2nk_0L + \varphi_r = 2\pi m \tag{1}$$

Here, n is the refractive index inside the cavity, $k_0 = 2\pi/\lambda_0$ is the modulus of the wave-

vector (related to the vacuum wavelength λ_0) φ_r is the phase-shift due to the reflection at the mirrors and m is an integer. In the idealized model used here, the phase shifts upon reflection at the two mirrors contribute a constant offset to the resonance condition, which we neglect [1].

When light enters the cavity at an angle θ , the resonances blue-shift because only the axial component of the wave-vector $k_z = k_0 \cos \theta$ contributes to the phase φ . Omitting φ_r , the phase-matching condition becomes [1]:

$$\varphi = 2nk_0L\cos\theta = 2\pi m\tag{2}$$

Due to θ changing k_z inside the cavity, we can find an angle $\theta(k_0)$ for every wavelength that enables resonance by modifying k_z to fit the condition equation 2 [9]:

$$\varphi(k_0, \theta) = 2nk_0 L \cos(\dot{\theta}(k_0)) = 2\pi m \tag{3}$$

Assigning a specific incidence angle θ to each wavelength in a broadband beam, such that shorter wavelengths enter at larger angles, can keep the axial component of the wave-vector k_z constant across the spectrum. Then, all wavelengths satisfy the resonance condition simultaneously, effectively removing the wavelength dependence of the phase, and achieving a flat, achromatic resonance [9]. This is illustrated in figure 1. Conventional dispersive elements like prisms and planar surface gratings are not suitable for achieving achromatic resonance in a cavity. Prisms don't produce enough angular dispersion, and gratings generate the wrong angle to wavelength relationship — longer wavelengths are refracted at larger angles, which conflicts with the resonance requirements. The system must instead generate an inverted, or "anomalous," angular dispersion, where shorter wavelengths are deflected more. We address this issue in section 3.

To better understand how resonance de-slanting works, we analyze how the axial component of the wave-vector k_z varies with wavelength and angle in a layer of a medium with refractive index n. We consider a broadband beam with a spectral bandwidth $\Delta\lambda$ centered at λ_c , where each wavelength λ_0 enters the layer at a different angle $\theta(\lambda_0)$ with regard to the incidence angle of the central wavelength ψ and an angular dispersion defined as $\beta = \frac{\theta(\lambda_0)}{\lambda_0 - \lambda_c}$, $[\beta] = {}^{\circ}/\text{nm}$. The axial wave-vector k_z for a wavelength λ_0 at angle θ is then given by [9]:

$$k_z(\lambda, \psi; \beta) = \frac{2\pi}{\lambda_0} \sqrt{n^2 - \sin^2(\psi - \beta \cdot (\lambda_0 - \lambda_c))}$$
 (4)

2.1 Experiment Design

To design a suitable experiment demonstrating achromatic resonance, some calculations have to be carried out. We first find the necessary angular dispersion. For this, we simulate the angular and spectral dependence of the axial wave-vector component k_z according to equation 4. Propagation takes place in air (refractive index n = 1) and our

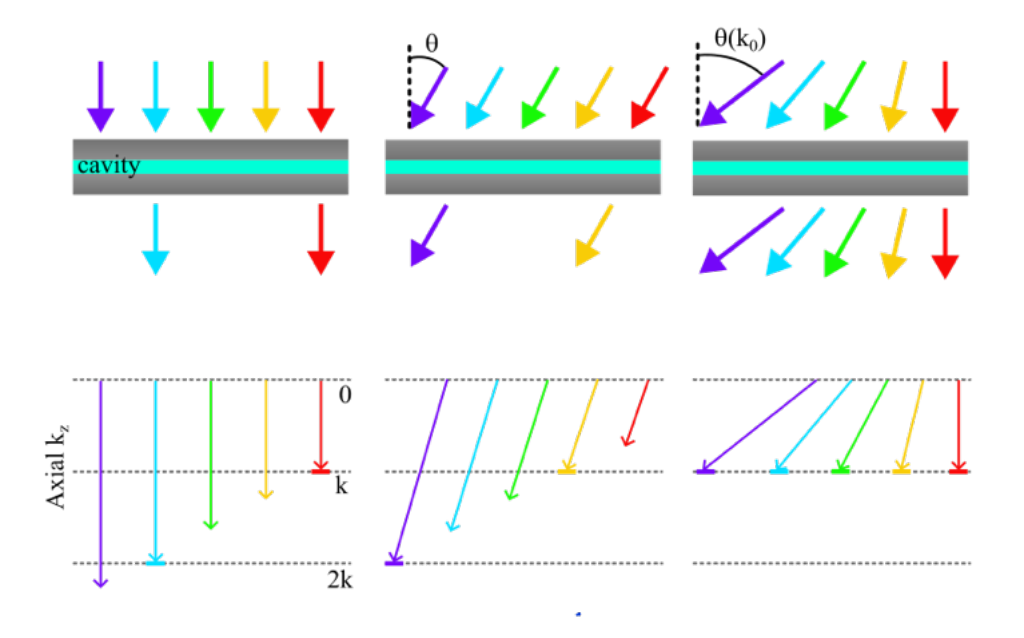


Figure 1: Broadbang light incident on the Fabry-Pérot cavity (top) comes in either normally, at an angle θ or at different angles depending the wavelength $\theta(k_0)$. For normal incidence, only certain wavelengths' axial wave-vector components k_z correspond to $k = \frac{m\pi}{L}$ (dashed lines in the bottom). When the light is incident at an angle θ , the resonances blue-shift. By assigning each wavelength λ_0 a corresponding angle of incidence $\theta(k_0)$, all wavelengths can simultaneously satisfy the resonance condition, resulting in achromatic transmission. Adapted from [9].

laser has a bandwith of $\Delta \lambda = 60$ nm around a central wavelength of $\lambda_c = 1030$ nm. We neglect the spectral dependence of n.

Figure 2 shows the $k_z(\lambda_0, \psi; \beta)$ for external angles of incidence ψ , from -60° to 60° .

The contour lines indicate constant values of k_z . The resonances of the cavity run parallel to these lines. The plot displays the behaviour for three different angular dispersions β . The first one, with $\beta = 0$ °/nm, represents the case in which the light is collimated and enters the cavity at different ψ . Increasing β slants the contours of constant k_z . The fact that this happens only for positive values of ψ is due to the need for anomalous angular dispersion, which appears for positive ψ , see 2.

Now, the angular dispersion can be adjusted until the desired behavior can be observed. We search for a value of β that de-slants the contour lines of constant k_z . This shows an independence of k_z from λ_0 over a certain spectral width, thus allowing for achromatic resonance to occur. Increasing β further causes the contours to slant so heavily that the dependence is over-corrected, and k_z varies with wavelength again.

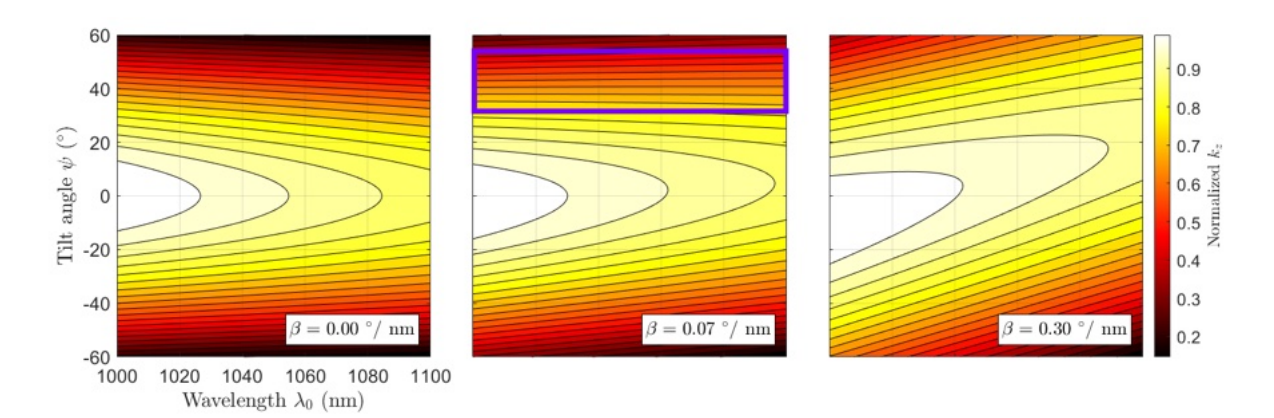


Figure 2: Contour plot of the Axial wave-vector component k_z as a function of tilt angle ψ and wavelength λ_0 for different angular dispersions β , normalized to $k_c = n \frac{2\pi}{\lambda_c}$. Contour lines show constant k_z values.

The blue box in the second plot marks an area with achromatic resonance in the cavity, i.e., where the value of k_z is independent of λ_0 for a range of wavelengths. The third plot shows over-correction caused by setting β too high.

We find that $\beta = 0.07$ °/nm is a suitable angular dispersion to enable achromatic resonance in the cavity. However, experimental limitations (see section 3), aggravated a measurement using this target β .

The rotation of the cavity introduces a lateral shift of the transmitted ray, which complicates the measurement of transmission through the cavity at tilt angles larger than 30°. Past this angle, the measured intensities drop and measurement resolution is reduced significantly. The transmitted bandwidth also decreases at angles of incidence away from 0°. Measured intensities outside of the wavelength range 1020-1040 nm are too small for proper depiction and interpretation (see figure 11). This bandwidth also further decreases when approaching higher ψ values.

These constraints require finding another target dispersion than the ideal case of $\beta = 0.07$ °/nm depicted in figure 2. Increasing β should allow reaching independence from λ_0 at lower ψ , at least for the measured bandwidth. A plot of k_z in the relevant wavelength and tilt angle range is depicted in figure 3.

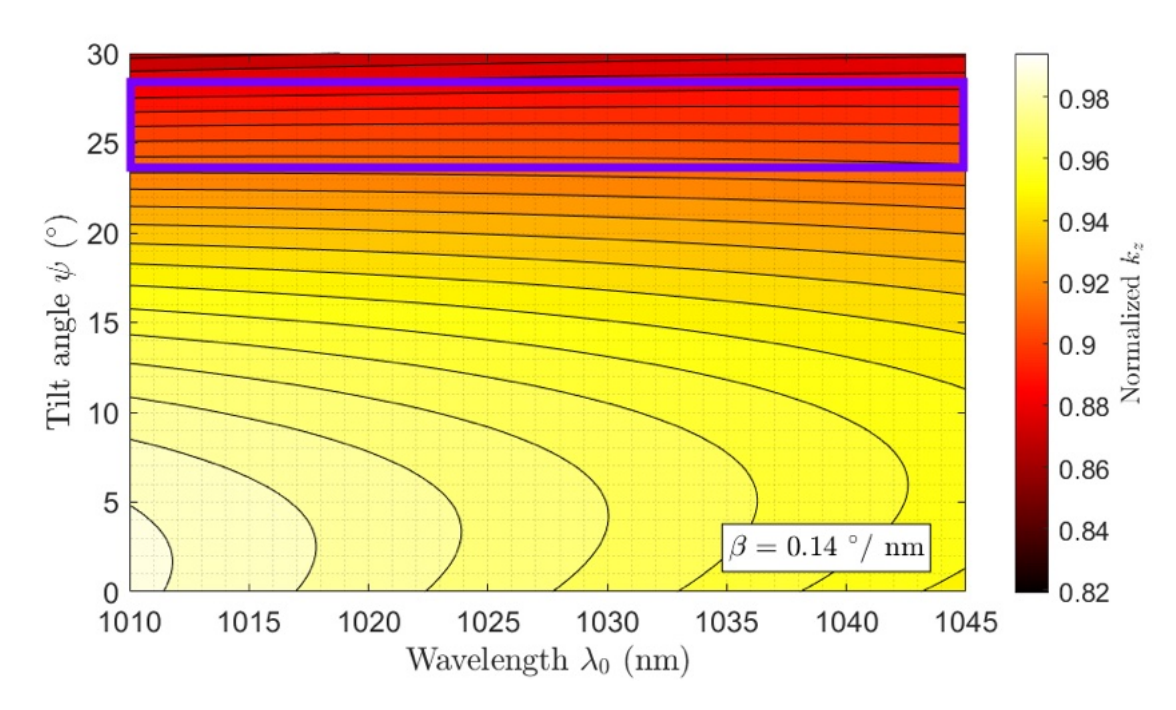


Figure 3: Contour plot of the axial wave-vector component k_z as a function of wavelength λ and tilt angle ψ for the wavelength range defined by the experimental setup. For a larger β the contours can be tilted such that, around $\psi = 25^{\circ}$, k_z becomes independent of λ_0 , enabling achromatic resonance in the cavity. (marked by the blue box.)

As figure 3 shows, achromatic resonance can be achieved by choosing the angular dispersion $\beta=0.14$ °/nm for $\psi=25$ °. This cannot be carried out with the same success for arbitrary ψ because the contours display a stronger curvature at smaller angles of incidence. This suggests that the bandwidth, over which achromatic resonance can be achieved, shrinks for small tilt angles. Choosing bigger β helps to "straighten" the contours, but at low angles their curvature predominates.

2.2 Reaching the Target Dispersion

In order to reach the angular dispersion required to see resonance independent of wavelength, two components have to be implemented into the experimental setup (see section 3). First, the laser beam is dispersed by a Thorlabs GTI25-03A transmission grating (d=300 grooves per millimeter [10]). Using

$$d(\sin \theta_c - \sin \alpha_c) = m\lambda_c,\tag{5}$$

with the vacuum central wavelength λ_c , the incidence angle α_c (for λ_c , measured from the surface normal, set to 0° in the experiment and calculations), the diffracted angle θ_c (for λ_c , measured from the surface normal) and the diffraction order m, yields an angular dispersion $\beta_{grating} = \frac{\partial \theta}{\partial \lambda} = 0.0181$ °/nm [11], around the central wavelength $\lambda_c = 1030$ nm for the first diffraction order. This is smaller than the target angular dispersion β required by section 2.1.

Using equation 5, the angle of the first diffraction order at the central wavelength λ_c is 17°.

In order to reach the required β , we use a convex lens to modify the light's angular dispersion before entering the cavity. It is important to note that this use of the lens is not based on the angular dispersion caused by the dispersive properties of the lens material, but by the lens' influence on the angular spread of incoming light rays: In the case of an existing angular dispersion, light of different wavelengths has a set angular spread per unit wavelength. This angular relation is then modified by the lens. The change can be calculated using the magnification M of the convex lens

$$M = -\frac{b}{a} = \frac{f}{f - a},\tag{6}$$

with the object distance a, image distance b and the focal length f [11]. Assuming normal incidence on the lens by the central wavelength and using the small angle approximation for the angular separation between two different wavelengths, the following relationship can be found:

$$\frac{\tan(\beta_f)}{\tan(\beta_i)} \approx \frac{\beta_f}{\beta_i} = \frac{h}{a} \cdot \frac{b}{h} = \frac{b}{a} = -M.$$

Here, h is the transverse separation of the wavelengths in the lens plane, β_i is the initial angular dispersion and β_f is the angular dispersion after passing through the lens.

This determines the change in angular dispersion due to a convex lens with a magnification M as

$$\beta_f = -\frac{1}{M} \cdot \beta_i = \frac{a - f}{f} \cdot \beta_i \tag{7}$$

The negative sign is due to the image being flipped by the lens. For f=35 mm and a target dispersion of $\beta=0.14$ °/nm, the required distance a between the grating and the lens is:

$$a = f \cdot \left(\frac{\beta}{\beta_{arating}} + 1\right) = 30.6 \text{ cm}$$
 (8)

Figure 4 shows a schematic of the change in angular separation through the lens.

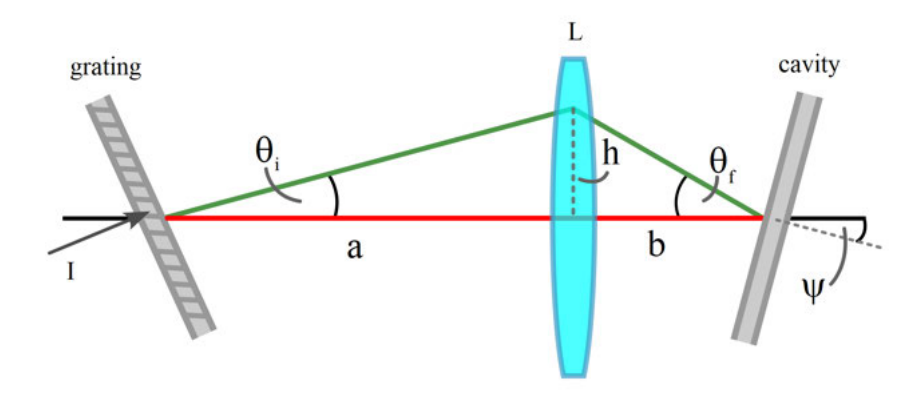


Figure 4: Schematic of the angular separation modification by the lens L. The incident ray I passes through the grating and gets diffracted. The angular separation between wavelengths after the grating, β_i , changes to an angular separation β_f after passing through the lens according to equation 7. The angle ψ marks the tilt of the cavity relative to the optical axis, that is defined along the diffracted ray of the central wavelength. The transverse separation between the two rays in the lens plane is denoted as h.

The distance from the lens to the cavity has no effect on the angular dispersion and was chosen such that the cavity does not coincide with lens focus.

3 Experimental Setup

The objective of the experiment is to confirm the theoretical calculations presented in section 2 and demonstrate omniresonance. As derived in section 2.1, achromatic resonance can be achieved in a Fabry-Pérot cavity by tailoring the angular dispersion such that the axial wave-vector component k_z becomes wavelength-independent. This is achieved by employing a setup that measures the spectral transmission at various angles of incidence ψ for a specific angular dispersion β of the incoming light beam.

Figures 5, 6 & 7 depict the experimental setup.

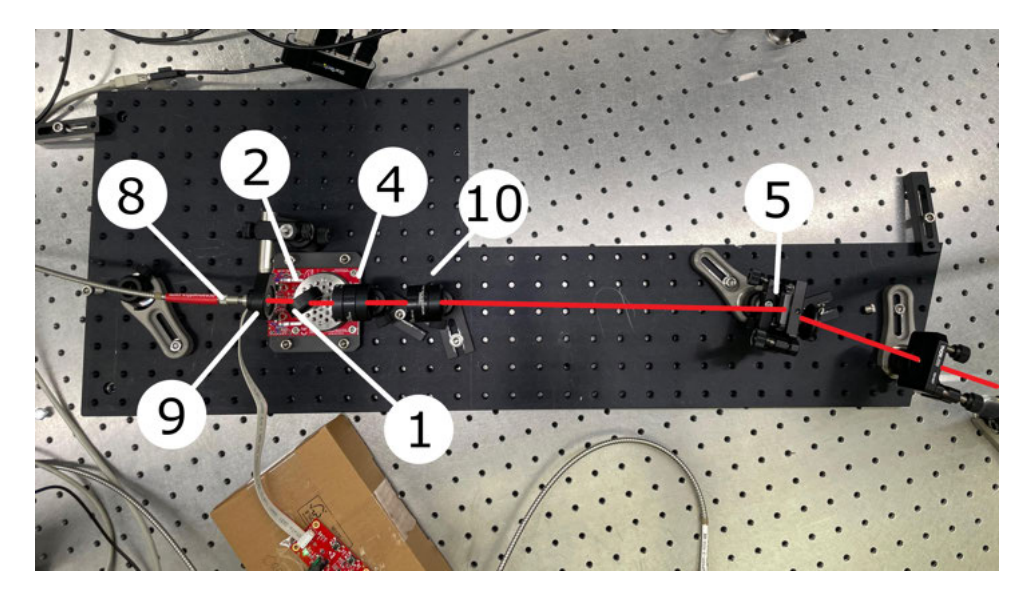


Figure 5: Top-down view of the experimental setup. The beam path is traced in red and components are marked with their respective numbers (see table 1).

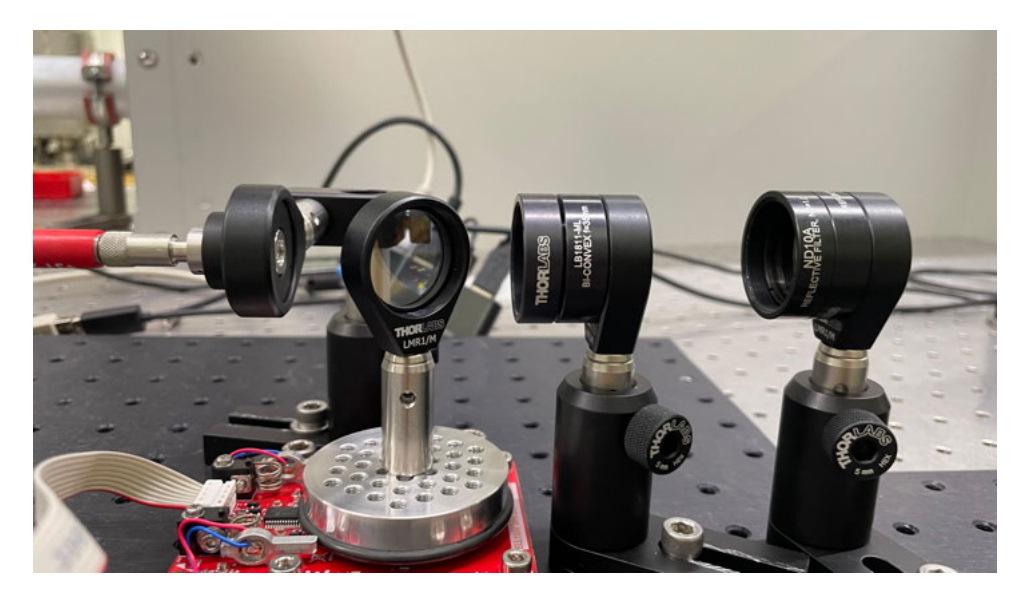


Figure 6: Side view of filters, lens, cavity and collimation. The cavity is rotated by 45° on the stage.

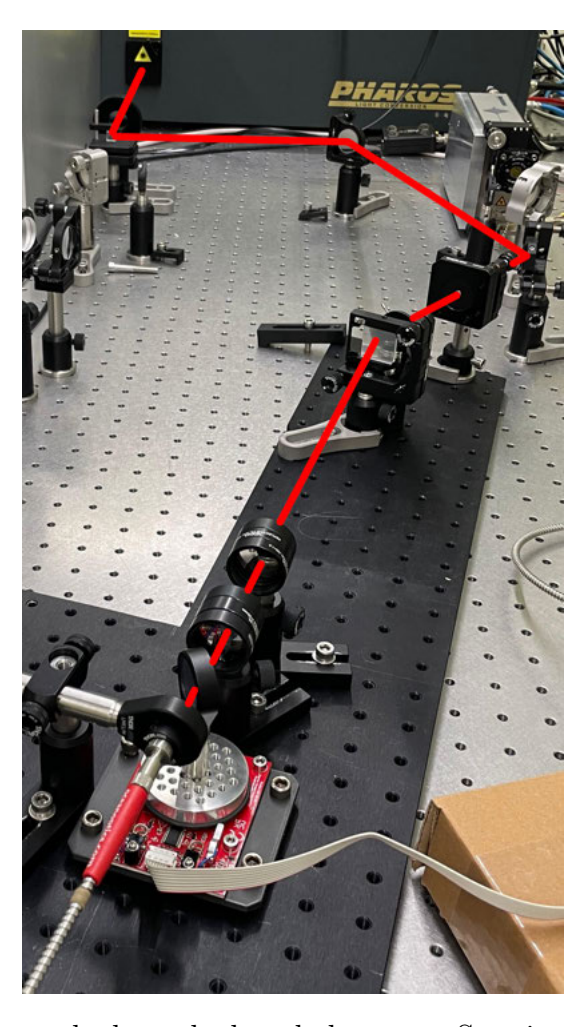


Figure 7: View of beam path through the whole setup. Starting at the laser and ending at the collimator.

The optical axis was chosen parallel to and 6.7 cm above the optical table's surface. Two mirrors, mounted on kinematic mirror mounts, are used to align the beam into the setup.

The laser used in the setup is a Light Conversion PHAROS femtosecond laser system. Its output was attenuated, with the spectrum centered at 1030 nm. The laser's broad spectral bandwidth allows for the simultaneous excitation of multiple cavity resonances (see figure 8). The pulse duration is not relevant to the measurements, as they focus on the cavity's spectral transmission.

The beam is aligned through an iris and then hits the grating at normal incidence. The first diffraction order appears rotated by 17° from the incidence angle. Three filters attenuate the intensity to prevent saturation of the spectrometer. A lens modifies the angular dispersion of the beam. After that, it enters the cavity, which is positioned behind the lens' focal length and aligned to the center of the rotation stage, to avoid clipping the beam upon rotation. A collimator then collects the transmitted light and couples it to a fiber, which delivers the light to the spectrometer.

The issue of anomalous diffraction is addressed by rotating the cavity relative to the incoming beam over a full angular range of 90° , starting from a tilt of -45° with respect

to normal incidence. This approach guarantees that, within the scanned range, either the positive or negative angular sector will produce the required anomalous angular dispersion relative to the cavity plane.

3.1 Components and Equipment

Table 1 provides an overview of the components and materials used in the experimental setup.

Table 1: List of components and materials used in the experiment, with their model, specifications and purpose. The column *No.* gives every component a number, by which it can be identified in the pictures.

Component	Model	Specifications and Purpose	No.
Cavity	Planar Fabry-Perot- Cavity	Consisting of 2 beam splitters and a spacer. (see section 3.2)	1
Rotation stage	Thorlabs $\mathrm{ELL18}(\mathrm{/M})$	Used to control the angle of incidence on the cavity (see ref. [12]).	2
Spectrometer	Avenir Aris Wide NIR	Measures the wavelength distribution of the light. Range: 300-1100 nm Resolution: 1.40 nm [13]	3
Lens	Thorlabs LB1811-ML Bi-convex lens	Focuses light and modifies the angular dispersion of the grating	4
Grating	Thorlabs GTI25-03A Transmission Grating	300 lines/mm.	5
Mirrors	-	Mirrors used to align the incoming beam.	6
Laser	Light Conversion PHAROS Femtosec- ond Laser	1000-1060 nm light source [14]	7
Optical fiber	-	Connects the optical output to the spectrometer.	8
Collimator	-	couples light to the optical fiber.	9
Filters	Thorlabs NDUV-A	ND filters reduce the light intensity before entering the cavity.	10

3.2 Construction and Characterization of the Cavity

The design of the cavity consists of two EKSMA Optics 032-7490S beam splitters and a spacer, sandwiched between the two beams splitters. The beam splitters are mounted with their reflective sides facing each other, so that the length L of the cavity is determined solely by the thickness of the spacer.

The spacer underwent multiple iterations in order to design a cavity with a suitable free spectral range (FSR). Initial constructions of the spacer ring had a thickness of 0.5 and 0.7 mm, resulting in an extremely small FSR, which made it difficult to resolve the interference pattern of the cavity with the spectrometer. As an alternative, the spacer ring was cut out of a 80 μm thick polyimide-film. Due to the inverse proportionality of the cavity length L and the FSR, this yielded a larger FSR, which made it easier to capture the interference pattern with the spectrometer.

The free spectral range ν_F , at normal incidence, can be calculated using

$$\nu_F = \frac{c}{2L},\tag{9}$$

with the speed of light in the cavity layer c and the length of the cavity $L=80~\mu\mathrm{m}$ (spacer thickness) [1]. Using the speed of light in vacuum c_0 and the refractive index of air n_{air} (assumed as wavelength-independent across the $\Delta\lambda$ spectral range), yields $\nu_F = \frac{c_0}{2n_{air}d} = 1.875~\mathrm{THz}$.

To confirm our cavity design, we measured the transitted intensity for multiple angles of incidence using the spectrometer. Figure 8 visualizes the cavity transmission at an incidence angle of $\psi = 0^{\circ}$.

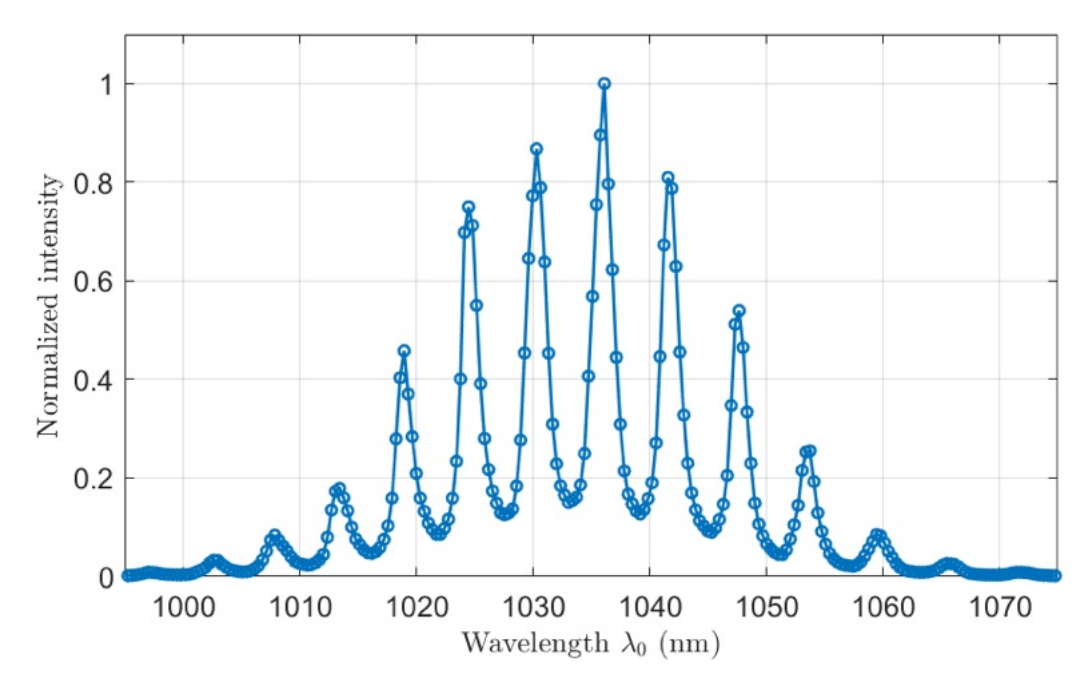


Figure 8: Transmission spectrum of the cavity for a tilt angle of $\psi = 0^{\circ}$. Measured data points are marked with circles. $\psi = 0^{\circ}$ corresponds to normal incidence on the cavity.

This measurement yields a cavity wavelength free spectral range λ_F (the distance between the first and last clearly identifiable peak divided by the number of peaks in between) of $\lambda_F = 5.71$ nm. Conversion of this wavelength spacing $\Delta\lambda$ into a frequency spacing $\Delta\nu$ then allows a comparison to the predicted FSR of the cavity:

$$\Delta \nu \approx \frac{c_0}{\lambda_c^2} \Delta \lambda = 1.613 \text{ THz}.$$

Using a central wavelength of $\lambda_c = 1030$ nm and the speed of light in vacuum c_0 . The result differs from the calculated FSR by 14%, possibly due to the mirror phase or a deviation of the spacer thickness.

3.3 Beam Splitter Characterization

The mirrors used are two EKSMA Optics 032-7490S Femtoline beam splitters designed for a target wavelength of 1030 nm. According to the manufacturer, they reflect $90\pm3\%$ and transmit $10\pm3\%$ of S-polarized light incident at an angle of $45\pm3^{\circ}$. As the intended use of the cavity is to examine transmission over multiple angles of incidence, we characterized the angle-dependent transmission of the beam splitters. This measurement is also used to normalize the cavity transmission: one beam splitter is mounted on the rotation stage instead of the cavity. Figure 9 shows the transmission through the beam splitter, measured with the spectrometer for incidence angles of -45° to $+45^{\circ}$. An angle of 0° corresponds to normal incidence.

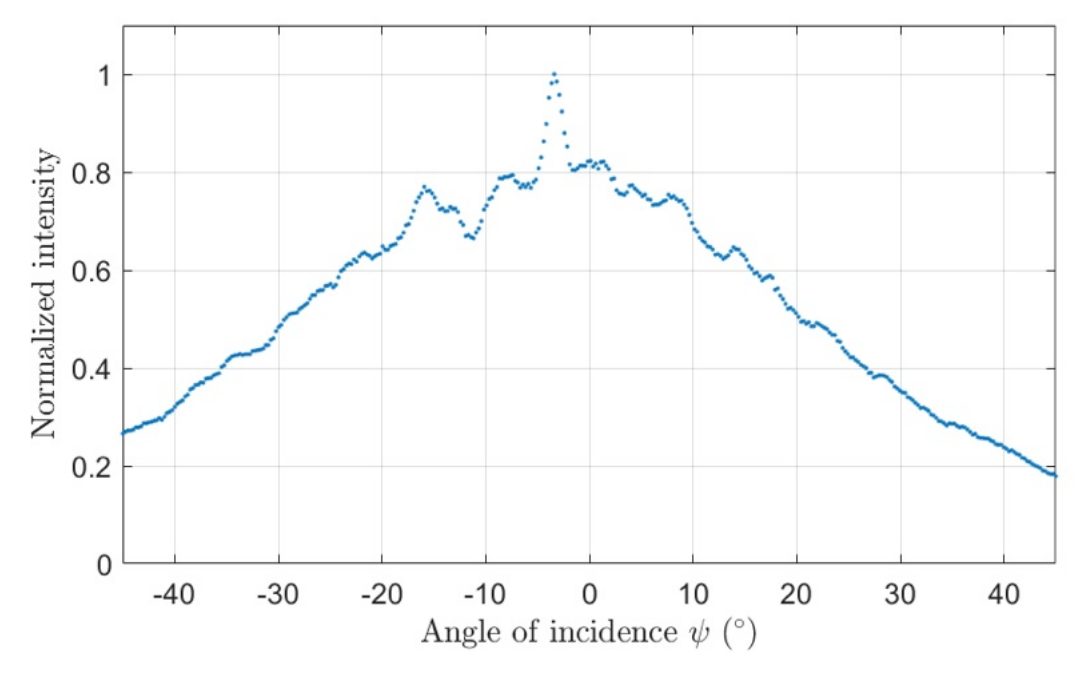


Figure 9: Transmission of the 032-7490S beam splitter versus incidence angle. Each data point represents the mean transmission in the 1000-1060 nm range at the angle of incidence ψ . The values are normalized the maximum mean transmission.

This does not give a completely accurate characterization for the transmission behavior of the beam splitter but a rough description of the transmission away from the intended angle of incidence.

4 Achromatic Resonance Demonstration

The goal of the measurement is to take the spectrum of the light transmitted through the cavity for a range of tilt angles ψ at a fixed angular dispersion β . The intensity is measured using an Avenir Aris spectrometer (see table 1). For this, we tilt the cavity over a range of ψ 's in increments of $\Delta \psi$. Each $\Delta \psi$, a spectrometer measures the complete spectrum of the transmitted light intensity (similar to figure 8). The exposure time is set to 55 ms.

First, when using no angular dispersion ($\beta=0^{\circ}$), the intensity transmitted through the cavity was measured for the relevant range of angles from $\psi=0^{\circ}$ to $\psi=45^{\circ}$ in steps of $\Delta\psi=0.25^{\circ}$ (see figure 10). This is the range in which anomalous angular diffraction is expected. Figure 10 plots the spectra as a heatmap depending on ψ and λ_0 . High intensities correspond to a fulfilled resonance condition.

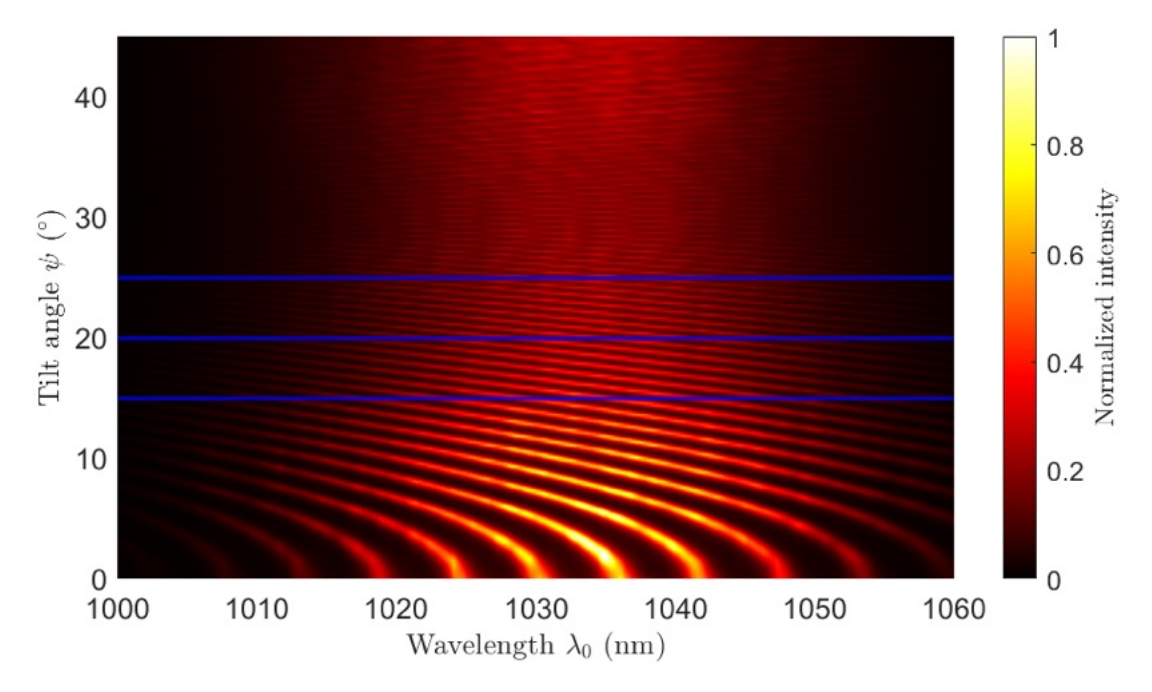


Figure 10: Intensity transmitted through the cavity for $\beta = 0^{\circ}$ versus ψ and λ_0 for a range of ψ from 0° to 45° . The blue horizontal lines provide a reference for the slant of the resonances.

The next measurement covers $\psi = -45^{\circ}$ to $\psi = 45^{\circ}$ with a step size of $\Delta \psi = 0.25^{\circ}$ for the target angular dispersion of $\beta = 0.14^{\circ}$. Figure 11 shows that the spectral transmission through the cavity has an overall narrower spectral width when introducing angular dispersion β (comp. figure 10). The resolution of the measurement is worse at larger angles of incidence and only the positive angular range causes anomalous diffraction,

so the negative range can be neglected when looking for de-slanting of the resonances. Therefore, we made another measurement with a smaller spectral and angular range but a higher angular resolution of $\Delta \psi = 0.125^{\circ}$.

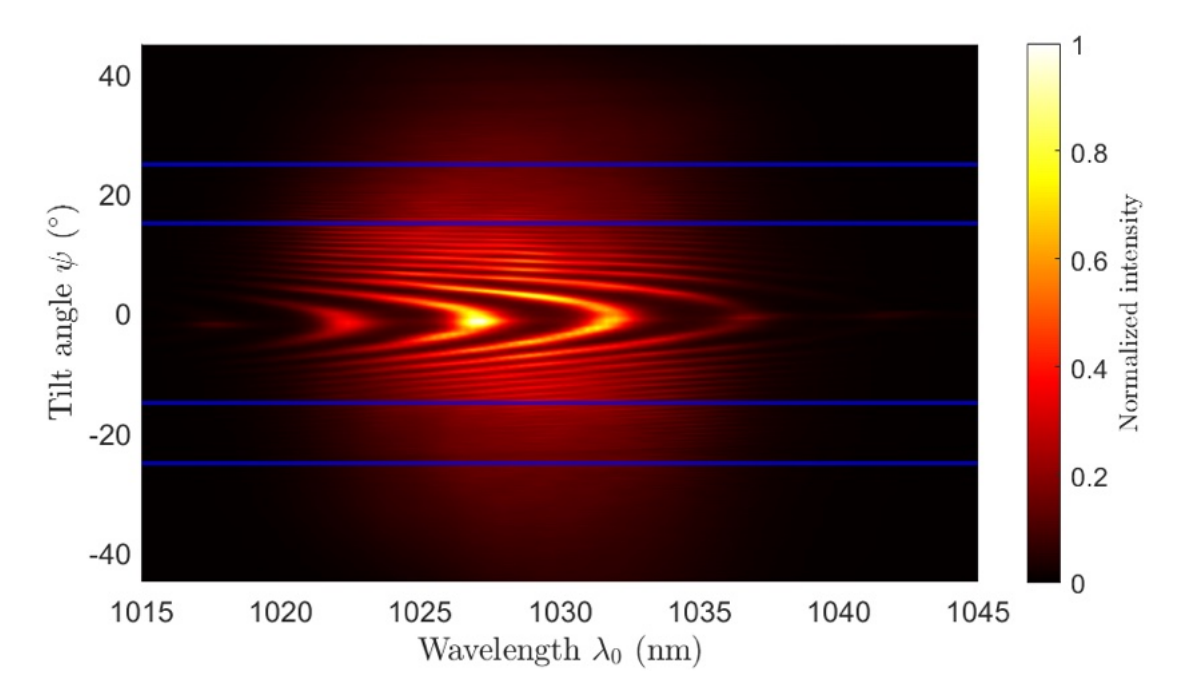


Figure 11: Measured spectral transmission through the cavity versus ψ and λ_0 . The intensity is normalized and horizontal lines provide a reference for the slant of the resonances.

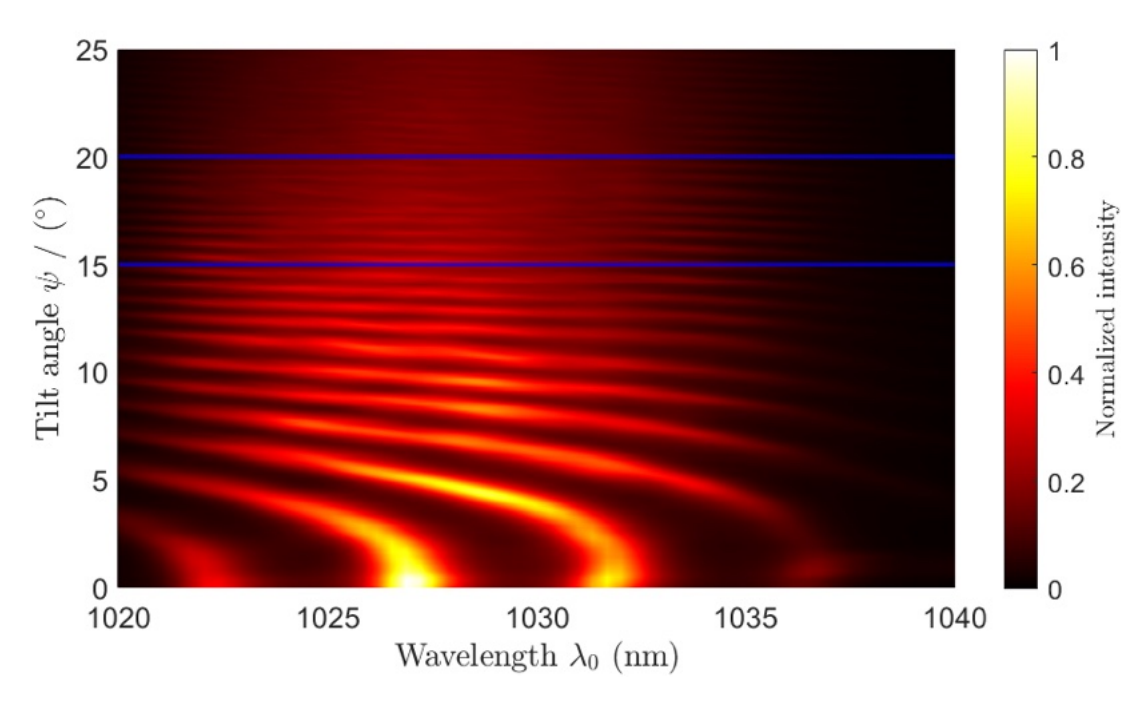


Figure 12: Measured spectral transmission through the cavity versus $\psi = 0^{\circ} - 25^{\circ}$ and λ_0 . The intensity is normalized. Horizontal lines give a reference for the slant of the resonances. In the range of 15° to 20°, the slant of the resonant features is reduced. This shows that the resonance condition becomes less wavelength dependent in this region when applying the target angular dispersion of $\beta = 0.14$ °/nm

The Measurement in figure 12 shows the de-slanting of the resonances in the marked angular range. This differs significantly from the angular range expected by figure 3. Nonetheless, the intensity stays independent of the wavelength over an extended spectrum spanning approximately 15 nm (about 3 times the FSR of the cavity). With this, achromatic resonance in the Fabry-Pérot cavity is achieved. To further illustrate this, figure 13 shows the spectrum of this measurement for selected ψ values.

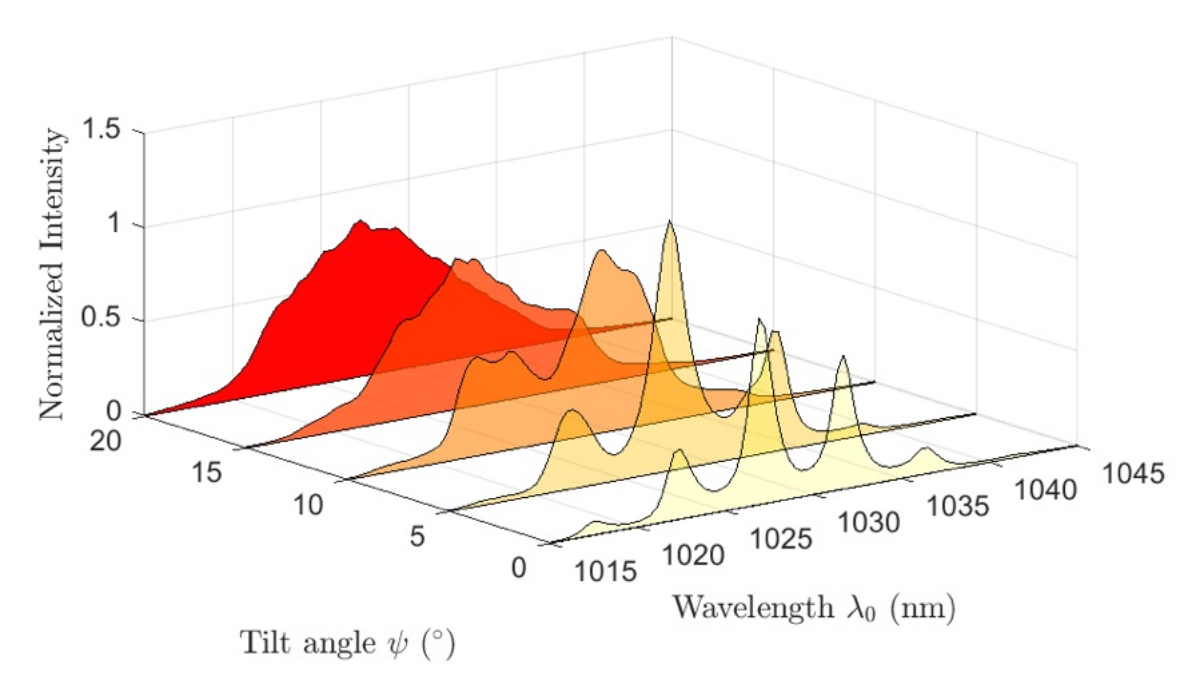


Figure 13: Spectrum of the transmission through the cavity for selected angles of incidence ψ . The intensities are normalized by the expected transmission through two beam splitters at the respective angle according to the measurement depicted in figure 9. The effect of achromatic resonance can be seen, with transmission of resonant wavelengths over multiple free spectral ranges.

This shows the effect of achromatic resonance in the cavity. At an incidence angle of $\psi=20^\circ$ the intensity does not show peaks at specific resonant wavelengths but over a broader spectrum ranging over multiple free spectral ranges of the cavity. Here, the wavelength dependence of the axial wave-vector component has been removed.

5 Discussion and Conclusion

The experimental results confirm key aspects of the theoretical model (see section 2.1) predicting achromatic resonance in a Fabry-Pérot cavity. By introducing a controlled angular dispersion of $\beta=0.14\,^\circ/\mathrm{nm}$, the wavelength dependence of the cavity's resonance condition was considerably reduced over a spectral range of 15 nm. This covers close to three spectral ranges of the Fabry-Pérot cavity used in the experiment.

Figure 12 shows this effect being at incidence angles ranging from $\psi = 15^{\circ}$ to $\psi = 20^{\circ}$. However, this differs from the angular range expected by the theoretical design of the experiment.

A number of possible sources for errors in the experimental setup could explain the behavior and need to be discussed:

The first possible error in the design arises from the distances between optical components,

especially the distance a between the grating and the lens (see equation 8). The modified angular dispersion β linearly depends on the distance a. Thus, an alignment error of 5 mm changes β by ± 0.008 °/nm. The actual angular dispersion after the lens was not measured during the experiment. As seen, when comparing figure 2 and figure 3, a change in β influences the angular and spectral range in which achromatic resonance can be achieved.

The lateral beam-shift caused by the rotation of the cavity with respect to the beam also presented a challenge during the measurement: The beam shifted at higher tilt angles. Thus, not the complete transmitted intensity reached the collimator, reducing the signal at higher tilt angles. The beam width at the collimator plane, assuming the target angular dispersion of $\beta = 0.14$ °/nm, measures 5.2 mm when the collimator lies 35 mm outside of the focal distance behind the lens. This narrows the measured spectra at high ψ because parts of the beam shift outside of the collimator lens. This could be circumvented by a piece of glass at the opposite rotation of the cavity that cancels the shift.

This experiment successfully demonstrates achromatic resonance in a Fabry-Pérot cavity using angular dispersion. The experimental design and measurement approach are based on the experiment by Soroush et al. [9], which explored the same effect for a different spectral range in the visible, requiring larger angular dispersion. In contrast to that work, the present experiment employs a transmission grating instead of a reflection grating and focuses on a spectral range from 1000 to 1060 nm. While the overall methodology remains similar, the setup had to be adapted to account for the different dispersive behavior and alignment requirements introduced by the new optical components. Despite deviations from the ideal theoretical predictions, the observed de-slanting of the resonance features confirms the feasibility of the method and validates the underlying model. Misalignment and optical losses, while non-negligible, did not prevent the appearance of the expected resonance-flattening.

A conceptually similar result has been achieved through entirely different means, such as in the work by Wicht et al. [7], where a white-light cavity is realized using atomic media to induce strong negative dispersion. While their approach modifies the material response inside the cavity, the method presented here achieves a similar achromatic effect through a geometric manipulation of the angular dispersion. Both techniques aim to cancel the wavelength dependence of the resonance condition and expand the usable spectral range of the cavity, showcasing different routes to the same fundamental goal.

STATUTORY DECLARATION

I declare that I have authored this thesis independently, that I have not used other than
the declared sources / resources, and that I have explicitly marked all material which has
been quoted either literally or by content from the used sources.

Graz, July 22, 2025		
(Signature)		

List of Figures

1	Resonance in the cavity at different incident angles	6
2	Contour plot of the axial wave-vector component k_z as a function of tilt the angle ψ and wavelength $\lambda_0 \ldots \ldots \ldots \ldots \ldots \ldots \ldots$	7
3	Contour plot of the axial wave-vector component k_z as a function of wavelength λ and tilt angle ψ for measurable wavelength range	8
4	Schematic of angular separation modification by the lens	10
5	Top-down view of the experimental setup	11
6	Side view of filters, lens, cavity and collimator setup	11
7	View of beam path through the whole setup	12
8	Transmission spectrum of cavity	14
9	Transmission of beam splitter over angular range	15
10	Normalized transmission intensity for $\beta=0^\circ$	16
11	Measured intensity transmitted through the cavity versus ψ and λ_0	17
12	Measured intensity transmitted through the cavity versus ψ and λ_0	18
13	Spectrum of the transmission through the cavity for selected angles of incidence	10

References

- [1] Bahaa E. A. Saleh and Malvin Carl Teich. "Fundamentals of Photonics, 3rd Edition". In: Hoboken: John Wiley & Sons, Inc., 2019. Chap. Resonator Optics, pp. 436–470. ISBN: 9781119506874.
- [2] Na Li et al. "Nonlinear all-optical switch based on a white-light cavity". In: *Phys. Rev. A* 93 (4 Apr. 2016), p. 043819. DOI: 10.1103/PhysRevA.93.043819. URL: https://link.aps.org/doi/10.1103/PhysRevA.93.043819.
- [3] Haibin Wu and Min Xiao. "White-light cavity with competing linear and nonlinear dispersions". In: *Phys. Rev. A* 77 (3 Mar. 2008), p. 031801. DOI: 10.1103/PhysRevA. 77.031801. URL: https://link.aps.org/doi/10.1103/PhysRevA.77.031801.
- [4] Kang Ying et al. "White light cavity via modification of linear and nonlinear dispersion in an N-type atomic system". In: Optics Communications 342 (2015), pp. 189-192. ISSN: 0030-4018. DOI: https://doi.org/10.1016/j.optcom. 2014.12.080. URL: https://www.sciencedirect.com/science/article/pii/S0030401814012449.
- [5] G Pati, Mary Salit, and S. Shahriar. "Demonstration of a Tunable-Bandwidth White-Light Interferometer Using Anomalous Dispersion in Atomic Vapor". In: *Physical review letters* 99 (Oct. 2007), p. 133601. DOI: 10.1103/PhysRevLett. 99.133601.
- [6] Jiepeng Zhang et al. "White-light cavity based on coherent Raman scattering via normal modes of a coupled cavity-and-atom system". In: *Phys. Rev. A* 81 (3 Mar. 2010), p. 033804. DOI: 10.1103/PhysRevA.81.033804. URL: https://link.aps.org/doi/10.1103/PhysRevA.81.033804.
- [7] A Wicht et al. "White-light cavities, atomic phase coherence, and gravitational wave detectors". In: Optics Communications 134.1 (1997), pp. 431-439. ISSN: 0030-4018. DOI: 10.1016/S0030-4018(96)00579-2. URL: https://www.sciencedirect.com/science/article/pii/S0030401896005792.
- [8] A. Wicht et al. "Experimental demonstration of negative dispersion without absorption". In: Optics Communications 179.1 (2000), pp. 107–115. ISSN: 0030-4018. DOI: https://doi.org/10.1016/S0030-4018(99)00528-3. URL: https://www.sciencedirect.com/science/article/pii/S0030401899005283.
- [9] Soroush Shabahang et al. "Omni-resonant optical micro-cavity". In: Scientific Reports 7 (Dec. 2016). DOI: 10.1038/s41598-017-10429-4.
- [10] NIR Transmission Gratings. (22.07.2025). Thorlabs GmBH. 2025. URL: https://www.thorlabs.com/newgrouppage9.cfm?objectgroup_id=1782&pn=GTI25-03#Intro.
- [11] Wolfgang Demtröder. "Experimentalphysik 2, Elektrizität und Optik, 7. Auflage". In: Berlin: Springer-Verlag GmBH Deutschland, 2017. Chap. Dünne Linsen. ISBN: 978-3-662-55789-1. DOI: https://doi.org/10.1007/978-3-662-55790-7.
- [12] Thorlabs, Inc. ELL18(/M) and ELL18K(/M) Rotation Stage and Rotation Stage Kits User Guide. Rev. D. Thorlabs. 2022. URL: https://www.thorlabs.com/.

- [13] Aris Spectrometer Product Sheet. (22.07.2025). Avenir Photonics GmbH & Co. KG. 2024. URL: https://www.avenirphotonics.com/wp-content/uploads/2024/05/datasheet_Aris_spectrometer_1.3.0.pdf.
- [14] Light Conversion. PHAROS Modular-Design Femtosecond Lasers for Industry and Science. https://lightcon.com/product/pharos-ultrafast-laser/. Revision 250606. Datasheet accessed July 2025. 2024.